Colloids and Surfaces A 598 (2020) 124810

Contents lists available at ScienceDirect

Colloids and Surfaces A

journal homepage: www.elsevier.com/locate/colsurfa

Combined microflotation of glass beads

N.N. Rulyov[a,b,*], L.O. Filippov[c,*], O.V. Kravchenko[a]

[a] Institute of Biocolloid Chemistry, National Academy of Sciences of Ukraine, Kyiv, Ukraine
[b] PV "TURBOFLOTSERVICE", Kyiv, Ukraine
[c] Université de Lorraine, CNRS, GeoRessources, F54000 Nancy, France

GRAPHICAL ABSTRACT

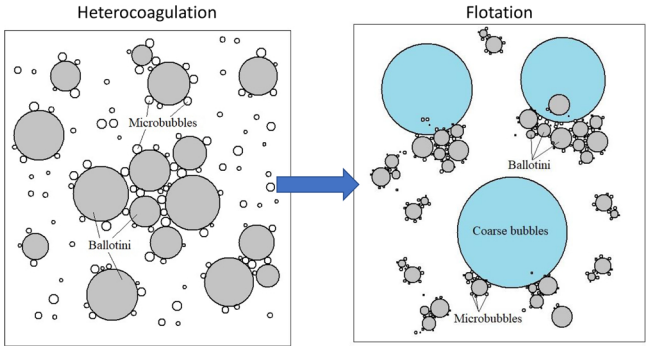

ARTICLE INFO

Keywords:
Combined microflotation
Air-in-water micro dispersion
Glass beads
Microbubbles

ABSTRACT

It is well established that application of microbubbles in combination with coarser ones ensures a significant increase in the flotation efficiency of very fine (< 20 μm) and very coarse (> 100 μm) particles. The objective of this study is to determine the impact of microbubbles on the flotation efficiency of medium-sized particles (50 − 80 μm). In tests runs we used glass beads (ballotini) of various size grades in the range:50; 50 − 63; 63 − 71; 71 − 80 μm as flotation objects. We used CTAB as both a collector and a frother at the dosage of 0.06 mg per 1 g of ballotini. Prior to starting flotation by coarse bubbles, a dosage of microbubbles less than 60 μm in size in the form of a concentrated (66 vol. %) microbubbles dispersion in CTAB solution of (0.2 g L^{-1}) produced by the MBGen-0.012 generator was fed into a flotation cell. The best flotation performance is observed for the fraction of 63 − 71 μm, whereas the flotation rate constants for all fractions are directly proportional to the volume dosage of microbubbles, when it does not exceed 0.2 mL g^{-1}. The size of microbubbles significantly affects the flotation effectiveness and depends on the concentration of the collector/frother used for their production. The main mechanism of flotation performance enhancement through microbubbles application, involves formation of coarse aggregates comprising large number of microbubbles and particles, which provides for a significant increase in the capture efficiency of aggregates by coarse bubbles.

1. Introduction

Flotation is one of the most efficient methods of ore and coal beneficiation. An essential precondition for a successful implementation of this technology is the feedstock comminution needed to separate a valuable mineral from gangue. This size reduction process leads to sufficiently wide particle size distribution ranging from several micrometers to several hundred micrometers. The flotation process involves

* Corresponding authors.
E-mail addresses: nrulyov@gmail.com (N.N. Rulyov), lev.filippov@univ-lorraine.fr (L.O. Filippov).

https://doi.org/10.1016/j.colsurfa.2020.124810
Received 25 January 2020; Received in revised form 14 March 2020; Accepted 1 April 2020
Available online 11 April 2020
0927-7757/

several sub-processes consisting in the interaction between particles and bubbles. The flotation rate constant and therefore the recovery is the results of the efficiency of the consecutive sub-processes such as particle-bubble collision (Ec), attachment (Ea) and stability of bubble particle aggregates (Es = 1-Ed) [1,2]. The separation of particles of a valuable component from gangue minerals is achieved through application of special reagents, which in the flotation process ensure selective attachment of particles of the mineral (or gangue), to the surface of rising bubbles. It is well known that the flotation rate significantly depends on the collision efficiency of particles by a rising bubble Ec, which in its turn depends on the ratio between the sizes of particle d_p and the bubble D_b [3–5]. The practice shows [6] that very fine particles (below 20 μm) and quite large ones (above 100 μm) float significantly worse compared to medium sized particles (in the range 50 − 80 μm). In the first case, this phenomenon is due to the fact that in the first approximation the value of Ec, is proportional to the square of the ratio d_p/D_b [7,8], which suggests that when, for example, the particle size decreases by two fold, floatability falls 4 fold. In the case of coarse particles, the critical factor that reduces the efficiency of their capture by a large bubble can be attributed to the high energy of their collision [9], and also to the high probability of particles detachment from a bubble surface under the impact of turbulent pulsations of the hydrodynamic field inside a flotation cell [10,11]. When a coarse particle collides with a large rapidly rising bubble, a sufficiently thick liquid film forms between them, but the collision time is too short to reduce the film thickness to a level when a thin film rupture appears, allowing a particle to attach to a bubble surface under the effect of surface forces. As a result, a particle bounces back from a bubble surface under the influence of the capillary forces acting from the side of a bubble surface, deformed by a particle impact. Calculations presented by Rulev et al. [9] show that for a coarse particle to get attached to a large fast rising bubble, a particle has to perform several consecutive jumps in order to dissipate the excessive kinetic collision energy.

One potential solution of the challenge of fine particles flotation involves the application of a technique, now termed as the combined microflotation, when alongside with coarse air bubbles flotation also employs relatively small amounts of microbubbles. As far back as the middle of the last century, it was found [12] that the introduction into pulp even relatively small amounts of microbubbles below 50 μm in size significantly accelerates flotation recovery of fine particles (below 20 μm) by relatively coarse bubbles (1 − 2 mm) produced in a flotation cell. Recently published papers [13–16] theoretically and experimentally substantiate the findings as in this case, microbubbles act as flotation carriers collecting on their surface fine particles, and then large bubbles float these aggregates, as it is shown in Fig. 1a. The recent research [17–19] have also demonstrated that the use of micro- and nanobubbles in combination with coarse bubbles boosts the flotation performance of coarse particles, larger than 100 μm. The studies show that when on the particles surface there are some well-settled micro- or nanobubbles, it is quite likely that colliding with a coarse bubble, a particle gets attached to a bubble due to the coalescence of small and coarse bubbles, as it is shown in Fig. 1b. Thus, in the flotation of coarse particles by large bubbles, microbubbles act rather as collectors than flotation carriers.

Based on the above, we can assume that application of micro- and nanobubbles in combination with coarse bubbles can significantly intensify the flotation not only of fine and coarse particles, but also of medium-sized ones. The objective of this study was to establish the effect of microbubbles on the kinetics of pneumatic-mechanical flotation of medium-sized particles simulated by glass beads (ballotini) of various size fractions.

2. Experimental

A suspension of glass beads (ballotini) produced by SWARCO-Vestglas served as a flotation object. Table 1 shows the chemical composition and the size distribution of flotation objects. The data indicate that the bulk ballotini (93.8 wt. %) comprise particles in the range of 50 − 71 μm.

Flotation tests were run on tap water using a laboratory pneumatic-mechanical flotation cell Mekhanobr-FM1M having a cell volume of 3 L and the cross section dimensions of 120 × 100 mm. The air flowrate was 1 L/min, and the rotor speed (diameter 60 mm) was 1000 rpm. The air was supplied by a controlled capacity peristaltic pump.

In all test runs, we used ballotini suspension in tap water; the suspension volume amounted to 3 L, with ballotini content of 0.1 kg. Cetyltrimethylammonium bromide (CTAB, $C_{19}H_{42}BrN$), produced by AppliChem GmbH (FRG) company was used both as a collector and a frother; its dosage in all experiments was 0.06 mg per 1.0 g of ballotini. It is worth to note that the collector used impacts not only the particle hydrophobicity but also the froth structure when the concenraion is varied in the experiments. Thus, overall flotaion results obtained include the effect of froth sability too. Microbubbles were produced by MBGen-0.012 unit, a generator of air-in-water microdispersion, made by Turboflotservice company (see Fig. 2). Microbubbles in the form of concentrated (66 vol. %) microdispersion of air in CTAB solution (0.2 g L^{-1}) were fed from the generator outlet into the flotation cell through a narrow PVC tube. The generator had the following capacity characteristics: for CTAB solution 1.9 mL s^{-1}, for microbubbles production up to 3.48 mL s^{-1}. Then these parameters, and the time for feeding the microbubbles dispersion into a flotation cell were used to calculate a volume dose of microbubbles per unit weight of ballotini and to define CTAB consumption in a flotation cell required to ensure that a total dose is equal to 0.06 mg g^{-1}.

1, 2-metering peristaltic pumps respectively for air and frother solution; 3–push button for air and frother solution metering pumps; 4-push button for disperser; 5 – disperser drive; 6 – instrument carry handle; 7– disperser head; 8 – pipe for air-in-water microdispersion discharge; 9 - pipe for feeding air-in-water mix into disperser head.

During the test runs ballotini suspension was placed in a flotation cell, then a required amount of CTAB was introduced into the cell with following mixing at a rotor speed of 1000 rpm but no air was supplied. After that, for a certain set pre-defined time, MBGen-0.012 generator fed an air-in-water micro-dispersion into the flotation cell, and after that the atmospheric air was supplied. Froth samples were collected in batches: 2 × 0.5 min and 2 × 1 min. Upon the completion of the flotation test, collected froth samples were filtered, dried and weighed. Numerical results shown graphically actually present the data averaged over three measurement runs. The relative measurement error comprises 2.5–3.4 %.

A laboratory unit, schematically shown in Fig. 3, was used to collect the data on the dispersity of microbubbles produced by the MBGen-0.012 generator. This unit allows to get micrographs of bubbles coming directly out of MBGen-0.012 generator into to the CTAB solution. In measurement runs, a peristaltic pump sucked in the microbubbles dispersion into a photographic cell. The photos were taken once the pump and the generator were switched off (and respectively the flow stopped). The procedure was repeated several times, and then the statistical processing of obtained images was performed. To estimate actual dimensions of bubbles, we used a calibrated tungsten filament of 35 μm of diameter placed inside the photographic cell.

The laboratory set schematically shown in Fig. 4 was used for obtaining visual information on aggregates consisting of microbubbles and ballotini particles, which were formed in a flotation cell upon the introduction of microbubbles into a cell. At the start of the measurements, ballotini suspension (10 g L^{-1}) in a CTAB solution (5 mg L^{-1}) was placed in a one-liter beaker. When mixing started, MBGen-0.012 generator was feeding microbubbles dispersion into the beaker for 2–3 s, after that the photos of the mixture were taken in the mode described above.

3. Results and discussion

Fig. 5 shows a typical micrograph of bubbles produced by MBGen-0.012 generator. Statistical processing of micrographs of this type

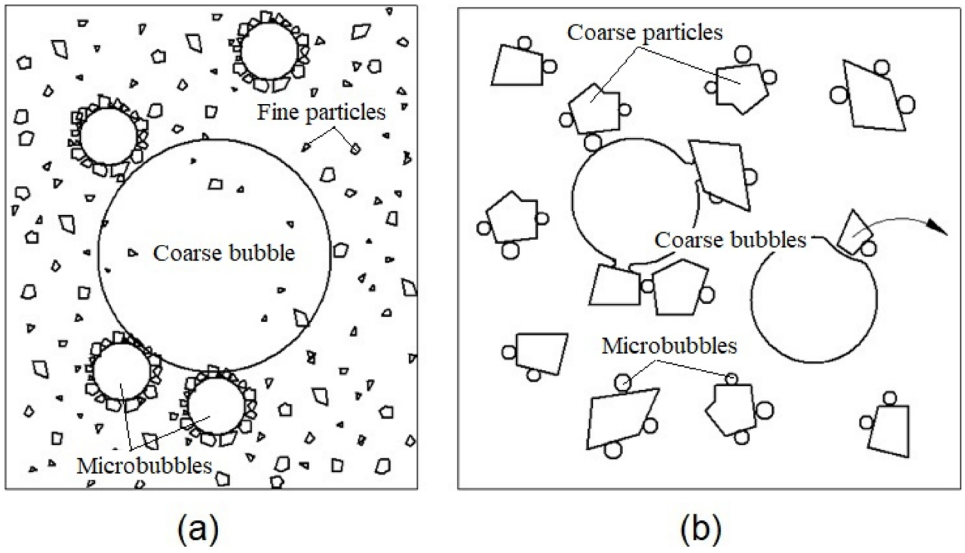

Fig. 1. Graphics explaining the role of microbubbles in the combined microflotation of fine (a) and coarse (b) particles. The arrow shows a rebound of a coarse particle from a coarse bubble in the absence of a microbubble between them at the collision.

Table 1
Chemical composition and size distribution of ballotini particles.

Chemical composition		Size distribution	
Chemical component	Content wt. %	Particle size μm	Content wt. %
SiO_2	> 65.0	+80	0.59
Al_2O_3	0.5 – 2.0	71 – 80	2.86
Fe_2O_3	< 0.15	63 – 71	69.02
MgO	> 2.5	50 – 63	24.76
CaO	> 8.0	40 – 50	0.55
Na_2O	> 14.0	33 – 40	1.05
Other	2.0	−33	1.17

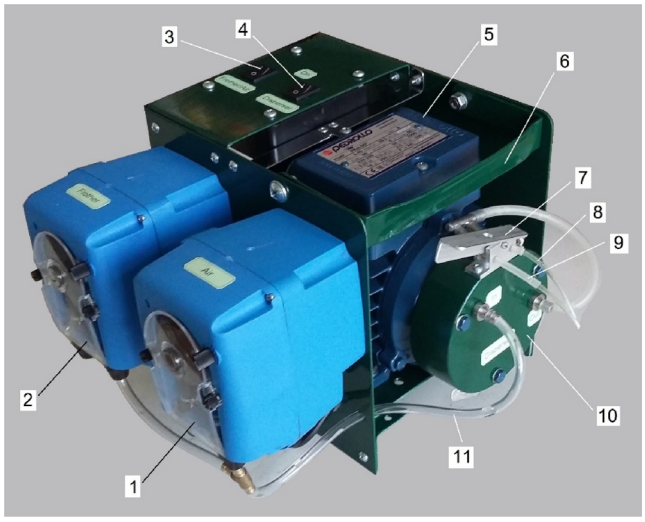

Fig. 2. Air-in-water microdispersion generator «MBGen-0.012».

allowed calculating the integral functions of bubbles size distribution. For illustrative purposes, Fig. 6 shows the distribution functions of bubbles received in the CTAB solution of the concentration of 0.1 and 0.2 g L^{-1} respectively. These findings demonstrated that at CTAB solution concentration of 0.2 g L^{-1}, 80 % of bubbles have size below 33 μm and 50 % - below 17 μm. When CTAB concentration decreases by two fold, these values increase respectively to 52 and 25 μm.

Obviously, when microbubbles get finer, the effectiveness of their application should increase. This is proven by the data on kinetics of ballotini recovery (71 – 80 μm) shown in Fig. 7, obtained for various concentrations of CTAB solution fed into the microbubbles generator. From Fig. 6 it follows that the increase in CTAB concentration and, hence, the decrease of microbubbles size leads to enhanced of both the flotation rate and the ultimate recovery.

Fig. 8 shows the flotation kinetics of the initial ballotini suspension at various dosage of CTAB in the absence of microbubbles, which demonstrates that at a dosage of 0.05 mg g^{-1} in 3 min almost 90 % recovery is achieved.

Based on the data shown in Figs. 6–8, in the major test runs on the combined microflotation we selected and further maintained following CTAB concentrations: 2 mg L^{-1} in the flotation cell; and 0.2 g L^{-1} in the solution used for microbubbles generation.

For studying the effects of microbubbles on the flotation kinetics of various particles size, the ballotini sieved into specific size fractions, in microns: < 50; 50 – 63; 63 – 71; 71 – 80, which were analyzed separately. Fig. 9 shows the recovery kinetic curves for different fractions in the absence of microbubbles and at a dosage of microbubbles of 0.23 mL g^{-1}, which demonstrate that for every fraction we can observe not only a significant increase in flotation rate, but also increased ultimate recovery.

Fig. 10 shows the dependence of flotation rate constants at the initial flotation time on the dosage of microbubbles for various fractions. The dependencies were calculated based on experimental data related to the recovery kinetics by the method of fitting the first-order reaction equation using the technique of least squares for the time interval 0 – 1 min. The obtained results show that for all fractions, the flotation rate constant is directly proportional to the microbubbles dosage in the range 0 – 0.20 mL g^{-1}. It is an interesting observation that similar results were obtained in the case of combined microflotation of finely dispersed quartz (−21 μm) [13], which were later theoretically substantiated in [15].

Thus, for small microbubbles dosage f for the flotation rate constant the following expression is valid

$$K(f) = K_0 + bf$$

where K_0 is the flotation rate constant at zero dosage of microbubbles, b is the proportionality coefficient.

Fig. 11 shows dependencies of flotation rate constants on the average particle size in fractions at different microbubbles dosage, which demonstrate that the maximum floatability is observed for

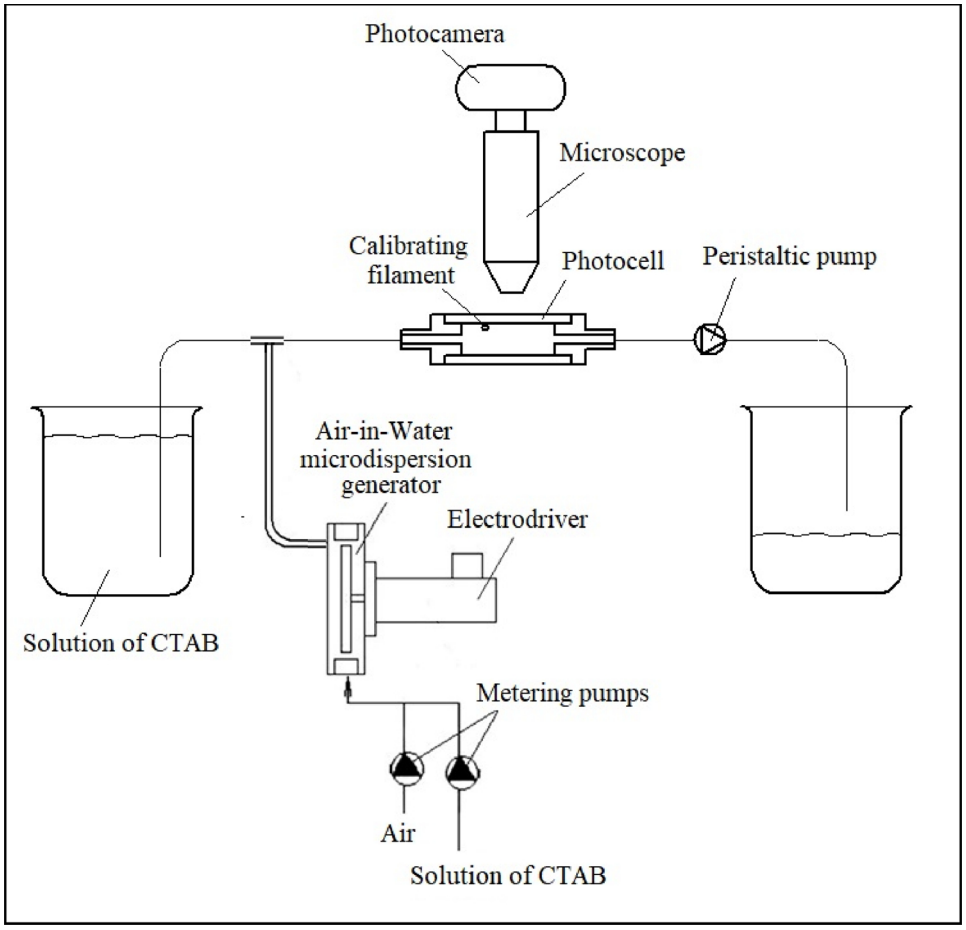

Fig. 3. Laboratory set layout for micrographing of bubbles produced by MBGen-0.012 generator.

particles in 63 − 71 μm fraction and the minimum floatability - for particles size in the fraction < 50 μm. For comparison, Table 2 presents the values of flotation rate constants at a zero dosage of microbubbles K_0, at a dosage 0.11 mL g^{-1} ($K_{0,1}$), as well as the values of the parameter b and the ratio $K_{0,1}/K_0$, that indicate that the largest relative increase in the flotation rate constant is observed for the smallest (< 50 μm) and largest (71 − 80 μm) fractions. At the same time, the largest value of the parameter b corresponds to the fraction

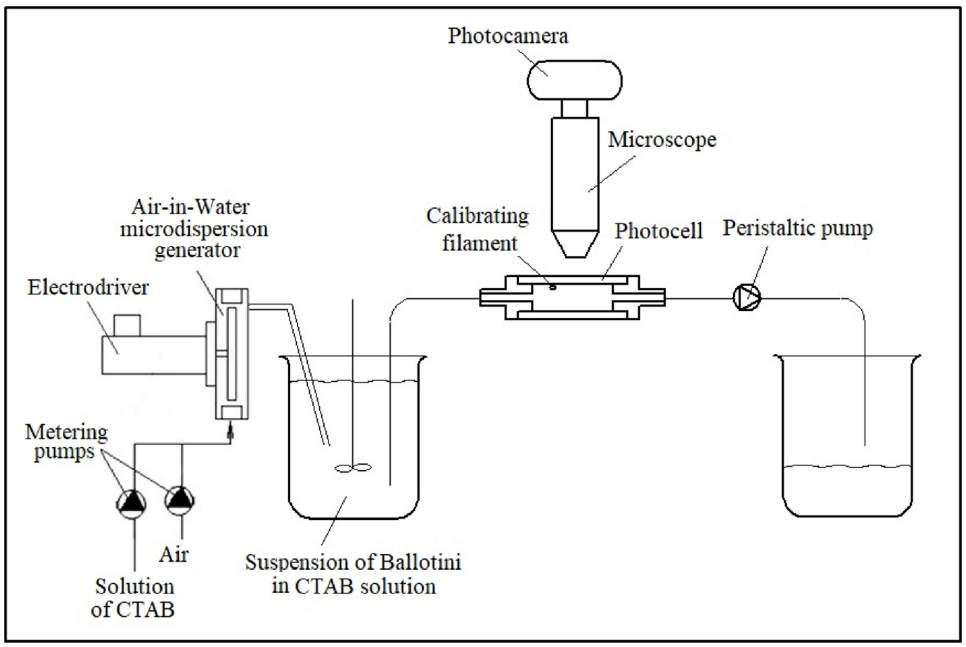

Fig. 4. Laboratory set layout for micrographing aggregates formed by ballotini and air microbubbles produced by MBGen-0.012 generator.

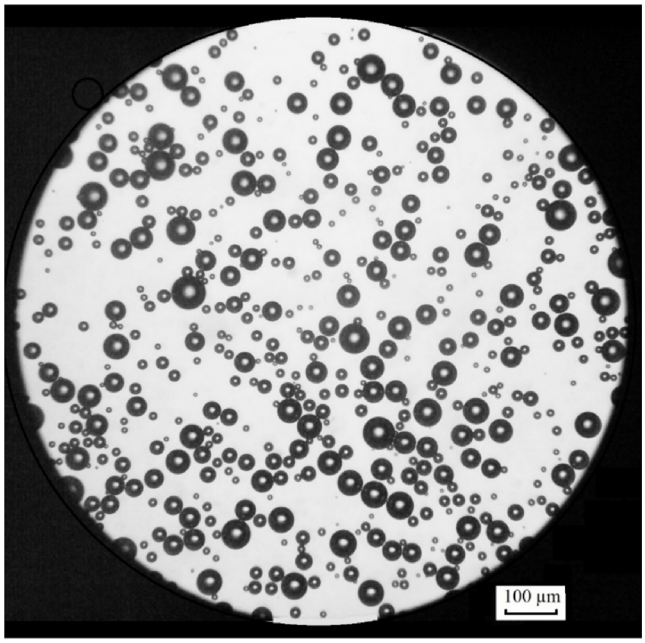

Fig. 5. Micrograph of bubbles produced by MBGen-0.012 generator in CTAB solution of 0.2 g L^{-1}.

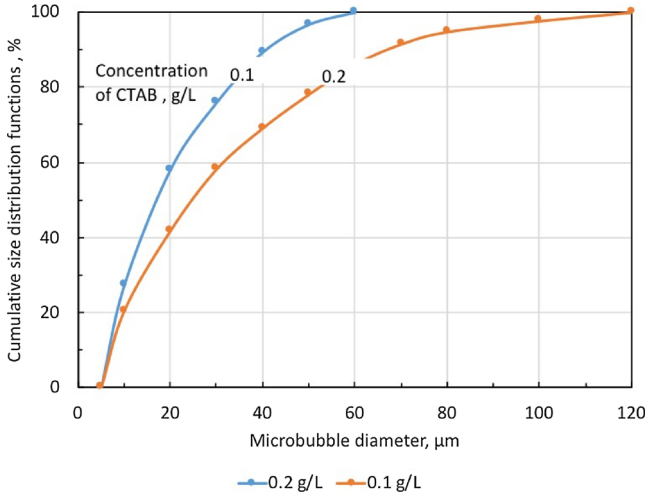

Fig. 6. Cumulative size distribution functions of bubbles produced by MBGen-0.012 generator in CTAB solution 0.1 and 0.2 g L^{-1}.

(63 – 71 µm), which has the highest floatability. The case that for medium-sized particles *b* parameter is significantly higher compared to that for coarse and fine particles can be attributed to the fact, that, "b" parameter refers to the flotation rate increase at low microbubbles dosage approaching zero. As coarse bubbles already nicely float medium-sized particles, even small amounts of microbubbles sufficiently enhance their flotation rate. In terms of fine and coarse particles, the enhancement in their flotation rate requires significant amounts of microbubbles. Hence, at higher microbubbles dosages the relative increase in their flotation rates is considerably greater compared to that for medium-sized particles.

These observations provided evidence that after microbubbles are fed into a flotation cell but before the start of air supply in the form of coarse bubbles, formation of aggregates occur which comprise ballotini particles and microbubbles, and the aggregate size increases with the increase of the microbubbles dosage. Thus, for example, at a microbubbles dosage of around 0.5 mL g^{-1}, the aggregate size was 3 – 5 mm, and naturally, after the supply of coarse bubbles into a flotation cell this

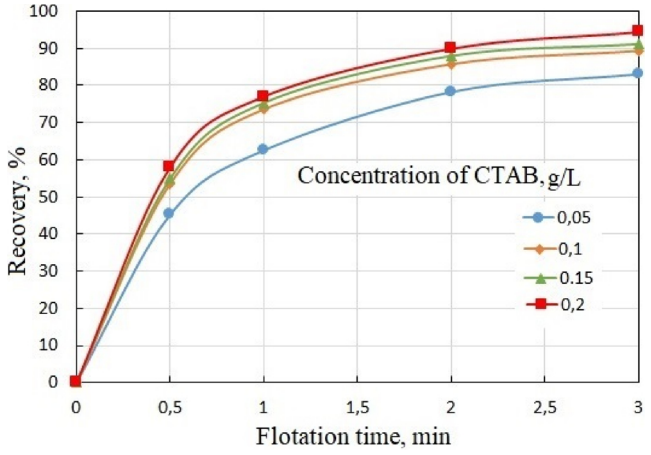

Fig. 7. Kinetics of ballotini (size fraction 71-80 µm) recovery for a microbubbles dosage of 0.23 mL per gram of ballotini and various concentrations of CTAB solution fed into the microbubbles generator. Total CTAB concentration in flotation cell – 2 mg/L.

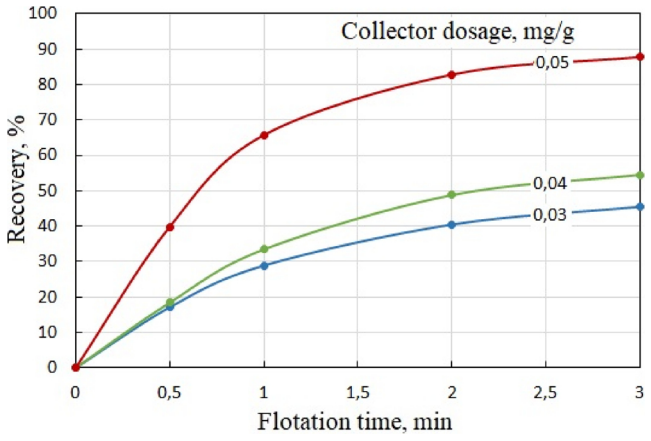

Fig. 8. Recovery kinetics of the initial ballotini suspension (– 90 µm) at different CTAB dosage in the absence of microbubbles.

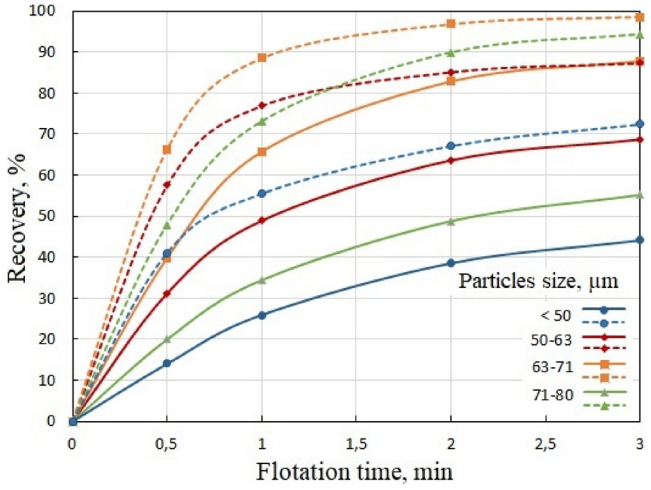

Fig. 9. Recovery kinetic of various ballotini size fractions without microbubbles application (solid lines) and at a microbubbles dosage of 0.23 mL/g (dashed lines). CTAB content in the solution fed into the microbubbles generator is 0.2 g L^{-1}.

significantly enhanced the flotation rate. As an illustration, Fig. 12 shows an aggregates micrograph taken by a unit schematically shown in Fig. 4; this photo clearly shows that each aggregate comprises several

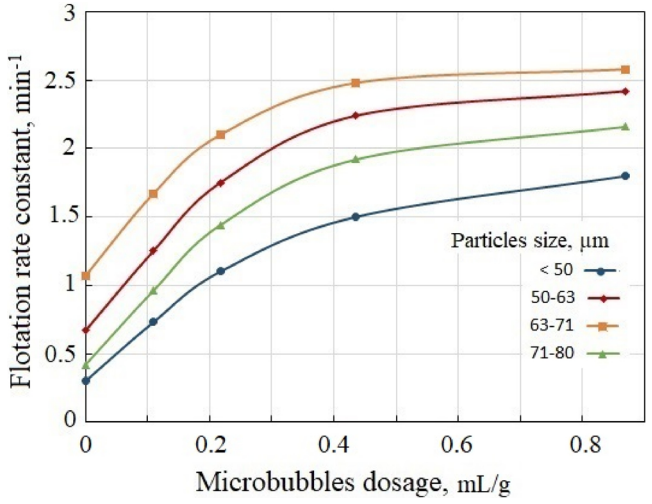

Fig. 10. Dependence of the flotation rate constant on the dosage of microbubbles at the initial moment of flotation.

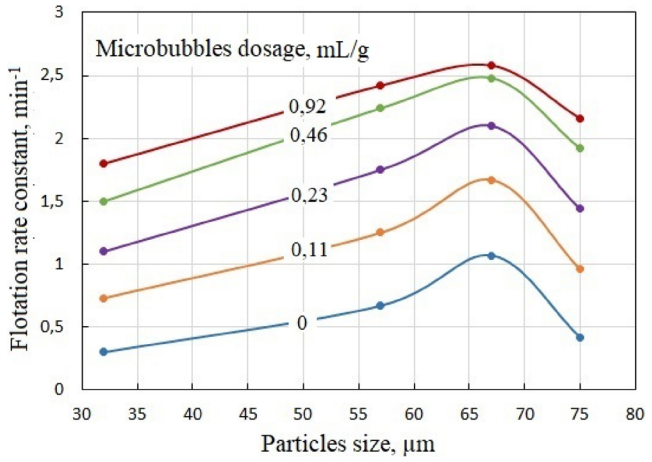

Fig. 11. Dependence of flotation rate constant on the mean size of particles in a fraction at various microbubbles doses.

Table 2
Ratio of flotation rate constants in the absence of microbubbles (K_0) and at the dosage of microbubbles 0.11 mL g^{-1} ($K_{0,1}$).

Size fraction, μm	K_0 min^{-1}	$K_{0,1}$ min^{-1}	$K_{0,1}/K_0$	b g mL^{-1} min^{-1}
< 50	0.3	0.72	2.40	3.82
50 – 63	0.67	1.25	1.86	5.27
63 – 71	1.07	1.67	1.56	5.45
71 – 80	0.42	0.96	2.28	4.91

microbubbles and multiple ballotini particles. In this test the ballotini content was decreased roughly by three folds compared to its content in flotation test runs in order to ensure better visual clarity of separate hetero aggregates.

Hence, we have every reason to argue that in the flotation of medium-sized particles, microbubbles act rather as flocculants than as flotation carriers or collectors. And since these aggregates are fairly large, they are floated comparatively well by coarse bubbles, as it generally shown in Fig. 13.

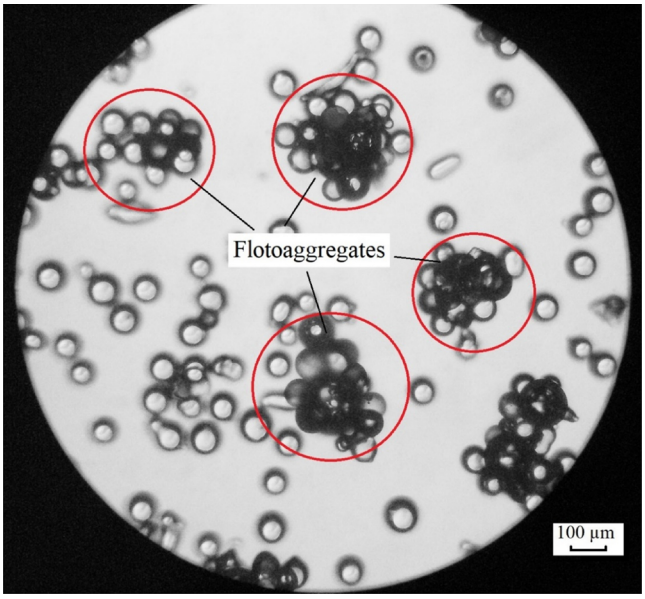

Fig. 12. Micrograph of flotation aggregates: light beads present ballotini, dark ones – microbubbles.

As the increased microbubbles dosage induces both aggregates growth in size and their better buoyancy, we can project that for sufficiently large dosage of microbubbles, it may be possible to exclude the use of coarse bubbles, as it is suggested by the principles of turbulent microflotation presented in [20–22]. However, in this case the microbubbles dosage should be significantly higher than 1 mL/g, which is required to ensure fast formation of aggregates, and their sufficient size, to provide for efficient separation of aggregates from the pulp and their transfer into the concentrate.

4. Conclusions

The above research findings suggest the following conclusions:

1 In flotation of medium-sized particles (50 – 80 μm) the application of microbubbles in combination with coarse bubbles provides for a significant increase in the flotation rate and the ultimate recovery.
2 The flotation rate constant is directly proportional to the volume dosage of microbubbles, when this dosage does not exceed 0.2 mL g^{-1}.
3 The size of microbubbles significantly influences the effectiveness of their application and depends on the concentration of a collector/frother used for their generation.
4 The principle mode of microbubbles action, which enhances the flotation efficiency, involves the formation of large aggregates formed by a large number of microbubbles and particles that ensures the significant increase in the efficiency of aggregates capture by coarse bubbles. Obviously, in an actual flotation system the effects of microbubbles, particle hydrophobiciy and froth stability could not be de-coupled when the collector used acts also as a frother.

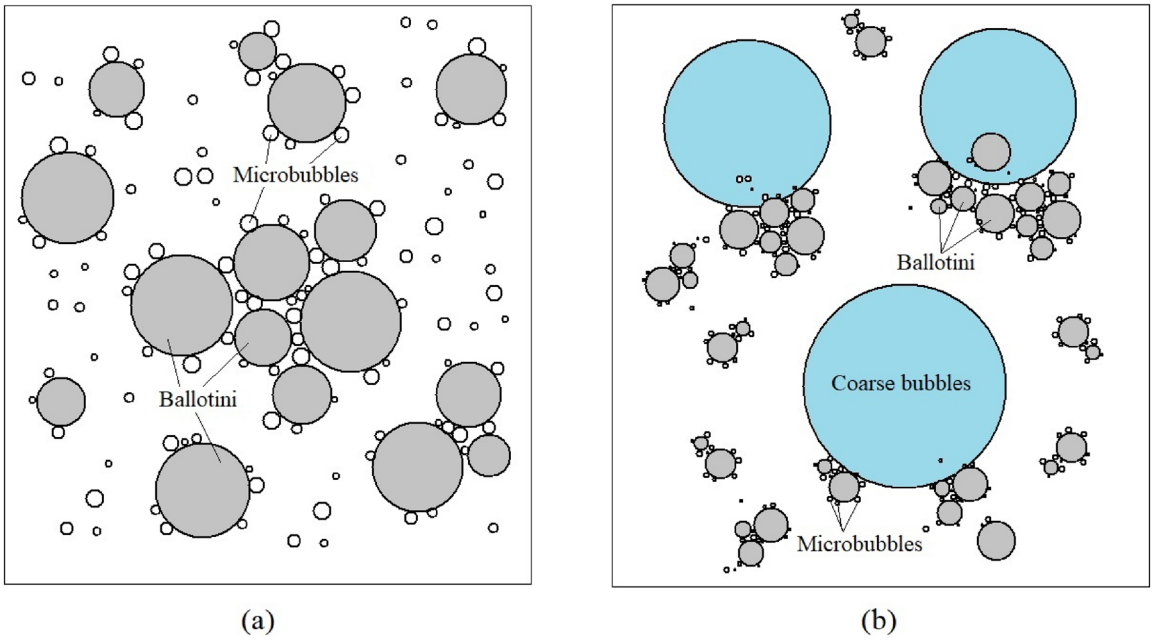

Fig. 13. Model of combined microflotation of ballotini, where microbubbles act as a flocculant: (a) – formation of ballotini/microbubbles aggregates; (b) – flotation of aggregates by coarse bubbles.

CRediT authorship contribution statement

N.N. Rulyov: Conceptualization, Methodology, Investigation, Writing - original draft. **L.O. Filippov:** Methodology, Data curation, Writing - review & editing. **O.V. Kravchenko:** Investigation, Visualization.

Declaration of Competing Interest

The authors declare that they have no known competing financial interests or personal relationships that could have appeared to influence the work reported in this paper.

Acknowledgments

This paper is supported by European Union's Horizon 2020 research and innovation programme under grant agreement No 821265, project Fine Future (Innovative technologies and concepts for fine particle flotation: unlocking future fine-grained deposits and Critical Raw Materials resources for the EU).

References

[1] B. Pyke, D. Fornasiero, J. Ralston, Bubble particle heterocoagulation under turbulent conditions, Colloid Interface Sci. 265 (1) (2003) 141–151.
[2] D. Fornasiero, L.O. Filippov, Innovations in the flotation of fine and coarse particles, J. Phys. Conf. Ser. 879 (2017) 012002.
[3] L.R. Flint, W.J. Hovarth, The collision efficiency of small particle with spherical bubbles, Chem. Eng. Sci. 26 (1971) 1135–1168.
[4] J.F. Anfruns, J.A. Kitchener, Rate of capture of small particles in flotation, Trans. Inst. Min. Metall. C: Miner. Process. Extract. Metall. 86 (1977) C9–C15.
[5] BV. Derjaguin, S.S. Dukhin, N.N. Rulyov, Kinetic theory of flotation of small particles, Plenum Press, Surface and Colloid Science. N. Y., London, 1984, pp. 71–113.
[6] W.J. Trahar, L.J. Warren, The floatability of very fine particles (review), Int. J. Miner. Process. 3 (1978) 103–131.
[7] D. Reay, G.A. Ratcliff, Removal of fine particles from water by dispersed air flotation, Can. J. Chem. Eng. 2 (1973) 178–185.
[8] D. Reay, G. Ratcliff, Effects of bubble size and particle size of collection efficiency, Can. J. Chem. Eng. 53 (1975) 481–486.
[9] N.N. Rulev, S.S. Dukhin, A.G. Chaplygin, Capture efficiency of floated particles during multiple inertial reflections, Kolloid Zhurn. 49 (1987) 939–948.
[10] H.J. Schulze, Hydrodynamics of bubble-mineral particle collisions. Mineral processing and extractive metallurgy, Trans. Inst. Min. Metall. C 5 (1989) 43–76.
[11] C.F. Gontijo, D. Fornasiero, J. Ralston, The limits of fine and coarse particle flotation, Can. J. Chem. Eng. 85 (2007) 739–747.
[12] V.A. Glembotzky, V.I. Klassen, Flotation, Moskau, Nedra, (1973).
[13] N.N. Rulyov, N.K. Tussupbayev, O.V. Kravchenko, Combined microflotation of fine quartz. Mineral processing and extractive metallurgy, Trans. Inst. Min. Metall. C 124 (2015) 217–233.
[14] N.K. Tussupbayev, N.N. Rulyov, O.V. Kravchenko, Microbubble augmented flotation of ultrafine chalcopyrite from quartz mixtures. Mineral Processing and Extractive Metallurgy, Trans. Inst. Min. Metall. C 125 (2016) 5–9.
[15] N.N. Rulyov, Combined microflotation of fine minerals: theory and experiment. Mineral Processing and Extractive Metallurgy, Trans. Inst. Min. Metall. C 125 (2016) 81–85.
[16] R. Ahmadi, D.A. Khodadadi, M. Abdollahy, M. Fan, Nano-microbubble flotation of fine and ultrafine chalcopyrite particles, Int. J. Min. Sci. Technol. 24 (2014) 559–566.
[17] M. Fan, D. Tao, R. Honaker, Z. Luo, Nanobubble generation and its applications in froth flotation (part IV): mechanical cells and specially designed column flotation of coal, Min. Sci. Technol. 20 (2010) 0641–0671.
[18] M. Fan, D. Tao, R. Honaker, Z. Luo, Nanobubble generation and its applications in froth flotation (part II): fundamental study and theoretical analysis, Min. Sci. Technol. 20 (2010) 0159–0177.
[19] S. Calgaroto, A. Azevedo, J. Rubio, Flotation of quartz particles assisted by nanobubbles, Int. J. Miner. Process. 137 (2015) 64–70.
[20] N.N. Rulyov, Turbulent microflotation: theory and experiment, Colloid Surf. A Physicochem. Eng. Asp. 192 (2001) 73–91.
[21] N.N. Rulyov, et al., Turbulent microflotation of fine disperse minerals (the general concept), in: J. Ralston (Ed.), In Proceedings of Strategic Conference and Workshop: FLOTATION & FLOCCULATION: From Fundamentals to Applications. (28 July-2 August 2002, Kailua-Kona, Hawaii), Snap Printing, Australia, 2003, pp. 177–184 2003.
[22] N.N. Rulyov, Turbulent micro-flotation of ultra-fine minerals. Mineral processing and extractive metallurgy, Trans. Inst. Min. Metall. C 117 (2008) 32–37.